CrossMark

PRECLINICAL STUDY

Host genetic modifiers of nonproductive angiogenesis inhibit breast cancer

Michael J. Flister[1,2,3] · Shirng-Wern Tsaih[1,2,3] · Alexander Stoddard[1] ·
Cody Plasterer[1,2,3] · Jaidip Jagtap[2,4] · Abdul K. Parchur[2,4] · Gayatri Sharma[2,4] ·
Anthony R. Prisco[3] · Angela Lemke[1,2,3] · Dana Murphy[1,2,3] · Mona Al-Gizawiy[2,4] ·
Michael Straza[2,5] · Sophia Ran[6,7] · Aron M. Geurts[1,3] · Melinda R. Dwinell[1,2,3] ·
Andrew S. Greene[3] · Carmen Bergom[2,5] · Peter S. LaViolette[2,4] · Amit Joshi[2,4]

Abstract

Purpose Multiple aspects of the tumor microenvironment (TME) impact breast cancer, yet the genetic modifiers of the TME are largely unknown, including those that modify tumor vascular formation and function.

Methods To discover host TME modifiers, we developed a system called the Consomic/Congenic Xenograft Model (CXM). In CXM, human breast cancer cells are orthotopically implanted into genetically engineered consomic xenograft host strains that are derived from two parental strains with different susceptibilities to breast cancer. Because the genetic backgrounds of the xenograft host strains differ, whereas the inoculated tumor cells are the same, any phenotypic variation is due to TME-specific modifier(s) on the substituted chromosome (consomic) or subchromosomal region (congenic). Here, we assessed TME modifiers of growth, angiogenesis, and vascular function of tumors implanted in the $SS^{IL2R\gamma}$ and $SS.BN3^{IL2R\gamma}$ CXM strains.

Results Breast cancer xenografts implanted in $SS.BN3^{IL2R\gamma}$ (consomic) had significant tumor growth inhibition compared with $SS^{IL2R\gamma}$ (parental control), despite a paradoxical increase in the density of blood vessels in the $SS.BN3^{IL2R\gamma}$ tumors. We hypothesized that decreased growth of $SS.BN3^{IL2R\gamma}$ tumors might be due to nonproductive angiogenesis. To test this possibility, $SS^{IL2R\gamma}$ and $SS.BN3^{IL2R\gamma}$ tumor vascular function was examined by dynamic contrast-enhanced magnetic resonance imaging (DCE-MRI), micro-computed tomography (micro-CT), and ex vivo analysis of primary blood endothelial cells, all of which revealed altered vascular function in $SS.BN3^{IL2R\gamma}$ tumors compared with $SS^{IL2R\gamma}$. Gene expression analysis also showed a dysregulated vascular signaling network in $SS.BN3^{IL2R\gamma}$ tumors, among which DLL4 was differentially expressed and co-localized to a host TME modifier locus (Chr3: 95–131 Mb) that was identified by congenic mapping.

Conclusions Collectively, these data suggest that host genetic modifier(s) on RNO3 induce nonproductive angiogenesis that inhibits tumor growth through the DLL4 pathway.

Keywords Breast cancer · Tumor microenvironment · Imaging · RNA sequencing · Genomics

✉ Michael J. Flister
mflister@mcw.edu

1 Human and Molecular Genetics Center, Medical College of Wisconsin, Milwaukee, WI, USA

2 Cancer Center, Medical College of Wisconsin, Milwaukee, WI, USA

3 Department of Physiology, Medical College of Wisconsin, 8701 Watertown Plank Rd., Milwaukee, WI 53226, USA

4 Department of Radiology, Medical College of Wisconsin, Milwaukee, WI, USA

5 Department of Radiation Oncology, Medical College of Wisconsin, Milwaukee, WI, USA

6 Simmons Cancer Institute, Southern Illinois University School of Medicine, Springfield, IL, USA

7 Department of Medical Microbiology, Immunology, and Cell Biology, Southern Illinois University School of Medicine, Springfield, IL, USA

Abbreviations

TME	Tumor microenvironment
CXM	Consomic Xenograft Model

Springer

DCE-MRI	Dynamic contrast-enhanced magnetic resonance imaging
SSRS	Species-specific RNAseq
PBST	Phosphate-buffered saline plus Tween-20
RNO3	Rat chromosome 3
TNBC	Triple-negative breast cancer
micro-CT	Micro-computed tomography
EC	Endothelial cell
DMEM	Dulbecco's modifier Eagle's medium
MFP	Mammary fat pad
RARE	Rapid acquisition rapid echo
IAUC	Initial area under the curve
ROI	Region of interest
FDR	False discovery rate

Introduction

Multiple nonmalignant cell types in the TME impact breast cancer risk and progression [1–4], yet the underlying heritable mechanisms that alter TME cell function and influence breast cancer outcomes are largely unknown. We developed CXM as the first strategy for mapping host TME modifiers [5]. In CXM, human breast cancer cells are orthotopically implanted into consomic and congenic xenograft host strains, which are derived from two parental strains with different susceptibilities to breast cancer (see Fig. 1a for schematic). Because the strain backgrounds are different, whereas the inoculated tumor cells are the same, any phenotypic variation is due to TME-specific modifier(s) that are localized to the substituted chromosome (consomic) or subchromosomal region (congenic), and can be elucidated by network-based expression analysis.

In the present study, we found that multiple breast cancer xenograft lines that were implanted into the consomic SS.BN3$^{IL2R\gamma}$ CXM strain had significant tumor growth inhibition compared with the parental SS$^{IL2R\gamma}$ strain, despite a paradoxical increase in tumor blood vessel density in SS.BN3$^{IL2R\gamma}$. Multiple clinical breast cancer studies have also correlated tumor vascular perfusion kinetics (i.e., tumor vascular function) with histopathologic prognostic factors [6], responses to neoadjuvant chemotherapy [7–10], and patient overall survival [11], leading us to hypothesize that TME modifier(s) on rat chromosome 3 (RNO3) might decrease tumor vascular function, which overrides the phenotypic effects of increased vascular density. Here, we characterized the growth and vasculature of triple-negative breast cancer (TNBC) tumors implanted in SS.BN3$^{IL2R\gamma}$ and SS$^{IL2R\gamma}$ rats using micro-CT, DCE-MRI, and in vitro morphometric analysis of primary blood vascular endothelial cells (EC). Additionally, species-specific RNAseq (SSRS) and quantitative immunofluorescent imaging were used to identify the potential TME modifier(s) that might alter tumor growth and vascular function. We found that SS.BN3$^{IL2R\gamma}$ tumors form a more tortuous and denser vascular network and have altered vascular function, which was similar to qualitative perfusion imaging in patients that had lower grade breast cancers [6] and improved 5-year overall survival [11]. The changes in the SS.BN3$^{IL2R\gamma}$ tumors also coincided with altered expression of DLL4, which was previously linked with nonproductive angiogenesis [12]. Moreover, DLL4 was co-localized within a host TME modifier locus (Chr3: 95–131 Mb) that was identified by congenic mapping and correlated with the phenotypic differences that were observed at the consomic level.
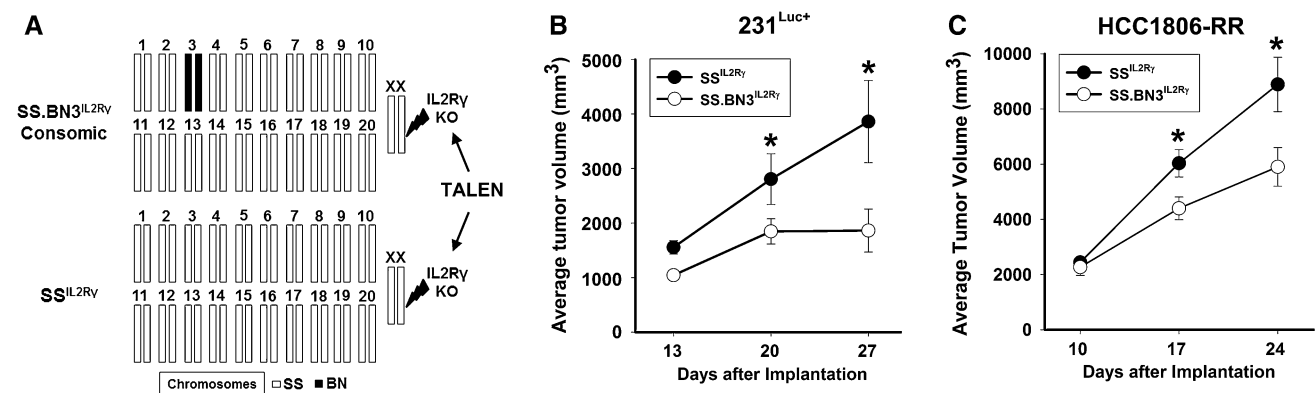

Fig. 1 Schematic of the SS.BN3$^{IL2R\gamma}$ and SS$^{IL2R\gamma}$ strains and tumor growth curves. **a** In CXM, the host genetic background is altered by one chromosome inherited from a different genetic background (*black bar*), enabling any phenotypic differences to be linked to the substituted chromosome (e.g., RNO3 in this case). **b** The growth of 231^{Luc+} tumors was monitored by caliper measurement at 13, 20, and 27 days post-implantation in SS$^{IL2R\gamma}$ ($n = 5$) and SS.BN3$^{IL2R\gamma}$ ($n = 7$) rats. **c** The growth of HCC1806-RR tumors was monitored by caliper measurement at 10, 17, and 24 days post-implantation in SS$^{IL2R\gamma}$ ($n = 8$) and SS.BN3$^{IL2R\gamma}$ ($n = 6$) rats. Data are presented as mean tumor volume $\pm$ SEM. *$p < 0.05$ as determined by a repeated measures ANOVA

Collectively, these data suggest that germline host TME modifier(s) of the pathways regulating tumor angiogenesis (e.g., the DLL4 pathway) might induce a switch from productive to nonproductive angiogenesis that inhibits breast cancer.

Materials and methods

Animals

All rats were provided food and water ad libitum and were housed at the Medical College of Wisconsin (MCW) Animal Resource Center. All procedures were approved by the MCW IACUC committee. The generation of the $SS^{IL2R\gamma}$ and $SS.BN3^{IL2R\gamma}$ rats has been described elsewhere [5]. Congenic strains were generated by crossing SS/Mcwi and the SS.BN3 consomic strain, followed by intercrossing the F1 progeny and F2 generation to capture different regions of RNO3 by marker-assisted selection, as described previously [13, 14]. Three new congenic strains were generated: line $A^{IL2R\gamma}$ [SS.BN-(D3Rat93-D3Mit3)/Mcwi], line $B^{IL2R\gamma}$ [SS.BN-(D3Rat26-D3Mgh18)/Mcwi], and line $C^{IL2R\gamma}$ [SS.BN-(D3Rat222-D3Rat218)/Mcwi].

Tumor implantation

The TNBC orthotopic models of firefly luciferase-tagged MDA-MB-231 (231^{Luc+}) cells and Renilla-tagged HCC-1806 (HCC1806-RR) were described previously [5, 15, 16]. Briefly, 231^{Luc+} cells (6×10^6) or HCC1806-RR cells (4×10^6) were suspended in 50% Matrigel and implanted into the #3 mammary fat pad (MFP) of female $SS^{IL2R\gamma}$ and $SS.BN3^{IL2R\gamma}$ rats. Tumor volume was determined by caliper measurements using the formula: volume $= Dd2\pi/6$, where D equals larger diameter and d equals smaller diameter.

DCE-MRI

The MRI study was performed on a 9.4T Bruker AVANCE Scanner fitted with a volume coil. The rats were anesthetized with 1.5% isoflurane and immobilized with a fiberglass bite-bar. Temperature was monitored and maintained at 37 ± 1.5 °C throughout the experiment. A RARE (rapid acquisition rapid echo) imaging sequence (TE/TR = 8/4 ms; matrix = 256 × 256; FOV = 3.5 cm, slice = 17.5 mm) was used to acquire sagittal scout images. A dynamically acquired T1-weighted spin-echo imaging sequence was acquired during the rapid injection of a gadolinium (0.1 mmol/kg Omniscan, Nycomed Amersham) contrast agent for a total of 5 min. Acquisition parameters included a TE/TR = 11/500 ms, matrix = 256 × 256, FOV = 3.5 cm, slice 1 mm, and phase repetition time of 6 s. Four coronal slices were chosen based on the RARE images and the tumor inoculation site. Pre- and post-T1-weighted spin-echo image were also acquired (TE/TR = 11/500 ms; matrix = 256 × 256; FOV = 3.5 cm; slice 2 mm) to delineate enhancing tumor. The DCE data were processed to generate initial area under the curve (IAUC), contrast washout, and initial slope images using the IB-DCE software plugin (Imaging Biometrics, Elm Grove, WI). Tumor and contralateral normal flank regions of interest (ROI) were drawn manually on the T1 + Gd images. Parameters were extracted from these ROIs for direct comparison between groups. The IAUC values were normalized by the contralateral flank values.

Micro-CT

Rats were completely perfused with saline containing 5 U/mL of heparin, followed by systemic injection of Microfil casting agent (Flow Tech, Inc., Carver, MA) and tissue processing, as described previously [17]. Micro-CT data were acquired on a Triumph SPEC/CT scanner (Gamma Medica-Ideas, Nortridge, CA) at a nominal resolution of 27 μm (65 kVp, 170 μA, 230-ms integration time, 2048 proj/180°, 28.9-mm-diameter field of view, 592 × 592 reconstruction matrix, cone-beam reconstruction. Gaussian smoothing and global thresh-holding procedures were applied to the grayscale data to contour the tumor (sigma = 2, support = 3, threshold = 30% of max grayscale value) and extract the tumor vascular network (sigma = 0.8, support = 1, threshold = 200% of max grayscale value).

Tube formation assay

Primary blood vascular endothelial cells (EC) were isolated using magnetic bead-conjugated anti-Pecam-1 antibodies (Cell Biologics; Chicago, IL) and cultured in DMEM containing 10% FBS and PenStrep. Four-chamber slides (Nunc Lab-Tek) were coated with 250 μL of matrigel (CB40234B, BD Biosciences) and allowed to solidify at 37 °C for 1 h, followed by seeding of 25,000 EC per well. After 24 h, images were acquired using a Nikon TS-100 Microscope equipped with a Flex camera (Nikon). Morphometric analysis of tube-like structures was performed using Pipeline [18].

Proliferation assay

EC were seeded in DMEM containing 1% FBS (control) or 10% FBS in 24-well plates at the density of 10,000 cells/well and incubated for 72 h. At 72 h post-seeding, EC were

trypsinized and enumerated using an automated cell counter.

Species-specific RNAseq

The SSRS method is outlined in Supplemental Fig. 1. Briefly, total RNA was extracted by Trizol from whole xenograft tumors that were excised from $SS^{IL2R\gamma}$ ($n = 4$) and $SS.BN3^{IL2R\gamma}$ ($n = 4$) rats, followed by library preparation using Illumina's TruSeq RNA library kit and sequencing on an Illumina HiSeq 2000. All raw sequencing data can be accessed from the Sequence Read Archive (https://www.ncbi.nlm.nih.gov/bioproject/PRJNA278049). A joint transcriptome reference file was produced by concatenating all the RNA sequences from human build GRCh38 and rat build Rnor5.0 and appending the coding sequence of firefly luciferase (GenBank accession U47295). Alignment and joint transcript abundance estimation, using the joint transcriptome reference, was performed for each separate xenograft sample with bowtie2 [19] and eXpress (version 1.5.1) [20]. Default parameters were used with the exception of a bowtie2 offset of 1, trading index size for increased alignment speed. An estimated counts table was compiled from all transcripts and samples and analyzed using the DESeq2 (version 1.4.5) [21] library for R. The rat and human (plus luciferase) transcripts were analyzed separately to allow for normalization of different relative contributions of malignant tumor cells and the nonmalignant host stroma. Differential expression values were estimated using individual transcript data and also at the gene level by first summing estimate counts across all alternative transcripts for each gene. This yielded transcript- and gene-level-estimated fold-changes and FDR-adjusted p values for human and rat transcripts separately (Supplemental Tables 1–4).

Immunofluorescent staining and measurement of mean fluorescent intensity

Immunofluorescent staining was performed using antibodies against CD31 (R&D Systems; AF3628 or BD; 555,025) and DLL4 (R&D Systems; AF1389), as described previously [5, 22]. Images were acquired at ×200 and 400 magnification on a Nikon E400 microscope equipped with a Spot Insight camera (Nikon Instruments).

Near infrared imaging of tumor vascular function

A bifurcated optical fiber bundle is used to deliver a 785 nm wavelength (power 75 mW, diode laser, Thorlab Inc.,) from two positions to uniformly excite the entire rat. A 16-bit deep cooled charge-coupled device (CCD) camera

(PI-XAM, Princeton Instruments) is used to image the rats through a computer-controlled WinView/32 software: first, the rat image with a 785-nm laser exposure and neutral density filter (OD = 4 at 785 nm) for 25-ms exposure to focus and align. For molecular imaging, a combination of 785-nm notch filter and 830 ± 10-nm bandpass filters was used on emission side and a series of 1500 frames having 256×256 pixels size (50-ms exposure time per frame and gain 10) were acquired in 5 min 43 s. Indocyanine green (ICG) was injected intravenously at 2 s after the image acquisition starts using a programmable syringe pump and the frames before ICG injection was used for the background correction.

Statistical analysis

Sigma Plot 11.0 was used to perform unpaired Student's t test. Chi-square, ANOVA, Fisher's exact, and Kolmogorov–Smirnov tests and empirical cumulative distribution plots for differential expression significance values were performed with R.

Results

Host TME modifier(s) of TNBC growth on RNO3 also elicit nonproductive angiogenesis

To assess tumor growth, 231^{Luc+} or HCC1806-RR cells were orthotopically implanted in the MFP of $SS^{IL2R\gamma}$ and $SS.BN3^{IL2R\gamma}$ CXM rats and tumor volumes were assessed by caliper measurement. Compared with 231^{Luc+} tumors implanted in $SS^{IL2R\gamma}$ rats at 27 days post-implant (3860 ± 754 mm^3, $n = 5$), $SS.BN3^{IL2R\gamma}$ tumors (1863 ± 395 mm^3, $n = 7$) were twofold smaller ($p < 0.05$) (Fig. 1b). Likewise, HCC1806-RR showed significant growth inhibition in $SS.BN3^{IL2R\gamma}$ rats (5904 ± 700 mm^3, $n = 6$) compared with $SS^{IL2R\gamma}$ rats (8893 ± 984 mm^3, $n = 8$) (Fig. 1c). These data demonstrate that TME-specific modifier(s) residing on RNO3 inhibit breast cancer growth [5].

Tumor growth requires vascular supply [23] and changes in vascular function are correlated with breast tumor grade [6] and overall survival [11], leading us to examine whether the TME-specific modifier(s) on RNO3 altered the tumor vasculature. Compared with $SS^{IL2R\gamma}$ tumors, the blood vasculature of TNBC tumors implanted in the $SS.BN3^{IL2R\gamma}$ genetic background was denser and more tortuous (Fig. 2a–e). Likewise, tumor blood vessel function differed between 231^{Luc+} tumors implanted in $SS.BN3^{IL2R\gamma}$ and $SS^{IL2R\gamma}$, as determined by DCE-MRI (Fig. 2f, g). Compared with $SS^{IL2R\gamma}$ tumors, the nIAUC was significantly higher in $SS.BN3^{IL2R\gamma}$ tumors ($p < 0.05$)

Fig. 2 Analysis of blood vasculature of TNBC tumors implanted in SS.BN3$^{IL2R\gamma}$ and SS$^{IL2R\gamma}$ rats.
a Immunofluorescent staining of CD31$^+$ blood vessels of 231^{Luc+} implanted in SS$^{IL2R\gamma}$ ($n = 5$) and SS.BN3$^{IL2R\gamma}$ ($n = 5$) rats. **b** Quantification of CD31$^+$ tumor blood vessels per 200× field ($n = 3$ fields per tumor). Data are presented as mean ± SEM.
**c** Immunofluorescent staining of CD31$^+$ blood vessels of HCC1806-RR implanted in SS$^{IL2R\gamma}$ ($n = 8$) and SS.BN3$^{IL2R\gamma}$ ($n = 6$) rats.
d Quantification of CD31$^+$ tumor blood vessels per 200× field ($n = 3$ fields per tumor). Data are presented as mean ± SEM. **e** Micro-CT reconstructions of the vascular networks of 231^{Luc+} tumors implanted in SS$^{IL2R\gamma}$ and SS.BN3$^{IL2R\gamma}$ rats.
f Representative T1 + Gd and nIAUC images from 231^{Luc+} tumors implanted in SS.BN3$^{IL2R\gamma}$ and SS$^{IL2R\gamma}$ rats.
g Plot of dynamic flow curves ($n = 6$ rats per group). **h** Bar charts showing the comparison of nIAUC and **i** washout of Gd contrast agent from tumor regions of interest. Data are presented as mean normalized values ± SEM. *$p < 0.05$ as determined by Student unpaired t test
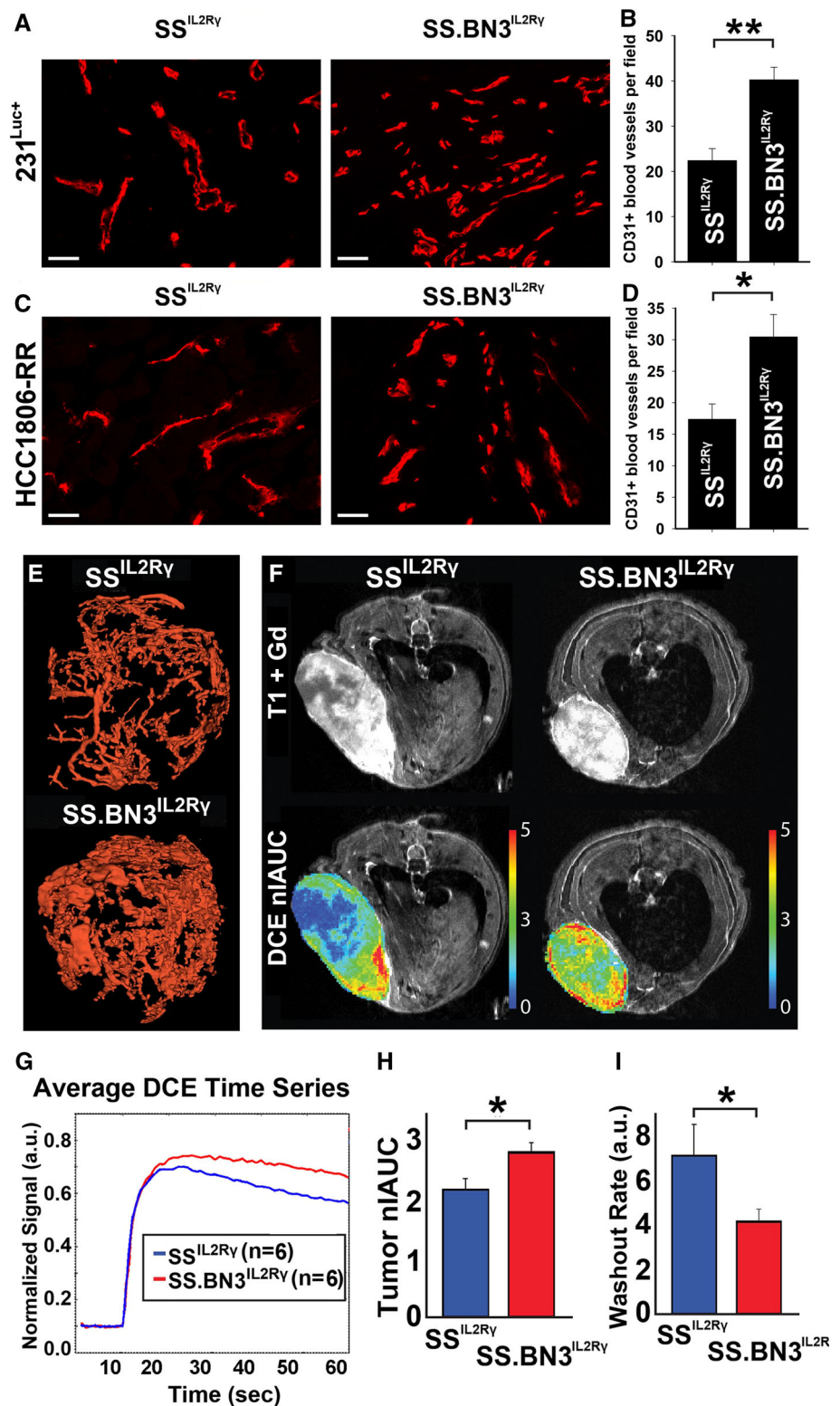
(Fig. 2h), demonstrating that SS.BN3$^{IL2R\gamma}$ tumors have increased total blood volume compared with SS$^{IL2R\gamma}$ tumors. The increased tumor blood volume might be explained by the higher density of tortuous blood vessels in tumors implanted in SS.BN3$^{IL2R\gamma}$ compared with SS$^{IL2R\gamma}$, as determined histologically (Fig. 2a–d) and by micro-CT (Fig. 2e). Moreover, the rate of washout of gadolinium contrast agent from SS.BN3$^{IL2R\gamma}$ tumors was significantly

lower than $SS^{IL2R\gamma}$ ($p < 0.05$, Fig. 2i), indicating that outward blood flow is slower in $SS.BN3^{IL2R\gamma}$ tumors and subsequent blood pooling could result in the higher peak total blood volume. Collectively, these data suggest that $SS.BN3^{IL2R\gamma}$ tumors have more disordered vasculature that functions differently than the $SS^{IL2R\gamma}$ parental strain and possibly contribute to delayed tumor growth in the $SS.BN3^{IL2R\gamma}$ rat.

One possible explanation of the altered vasculature in $SS.BN3^{IL2R\gamma}$ tumors is that genetic modifier(s) on the BN-derived RNO3 intrinsically alter EC function at the cellular level. To explore this possibility, we used an in vitro model of primary blood vascular EC derived from SS.BN3 consomic and SS rats to examine proliferative capacity and tube formation. As shown in Fig. 3a, b, isolated EC showed cobblestone morphology and expression of multiple vascular EC markers. The proliferative capacity of the SS.BN3-derived EC was significantly higher ($p < 0.05$)

compared with SS-derived EC (Fig. 3c). Likewise, the density of tube-like structures formed by SS.BN3-derived EC was significantly higher ($p < 0.001$) than SS-derived EC (Fig. 3d, e), despite the same number of EC being seeded per well. Further morphometric analysis revealed that SS.BN3-derived EC formed tube-like structures with significantly more branch points (Fig. 3f) and thinner tubes (Fig. 3g) compared with SS-derived EC. Collectively, these data suggest that the altered vasculature in $SS.BN3^{IL2R\gamma}$ tumors could be due to TME modifier(s) on RNO3 that directly alter EC function.

Host TME modifier(s) on RNO3 alter a vascular gene network

Species-specific RNAseq (SSRS) was used to identify host TME gene networks that were differentially expressed (DE; FDR < 0.1) in 231^{Luc+} tumors implanted in $SS^{IL2R\gamma}$

Fig. 3 Functional analysis of blood vascular endothelial cells (EC) derived from SS and SS.BN3 rats. a Morphology of EC derived from SS and SS.BN3 rats was identical between strains and resembled a cobblestone morphology that is characteristic of EC. Images were acquired at 200× and the scale bar represents 100 μm. b Purified ECs express blood endothelium markers. (+) indicates positive control RNA and (−) indicates a no template control. c Proliferative response of EC to serum. Data are presented as mean ± SEM ($n = 4$ per group). *$p < 0.05$ and **$p < 0.01$, as determined by ANOVA followed by the Holm–Sidak multiple comparison test. d Brightfield images of EC tube formation for SS ($n = 8$) and SSBN3 ($n = 8$). Images were acquired at 400× and the scale bar represents 500 μm. e Quantification of the total area of tube-like structures per 40× field. f Quantification of EC tube branch points per 40× fields. g Quantification of EC tube thickness per 400× field. Data are presented as mean ± SEM. *$p < 0.05$, **$p < 0.01$, and ***$p < 0.001$, as determined by Student unpaired t test
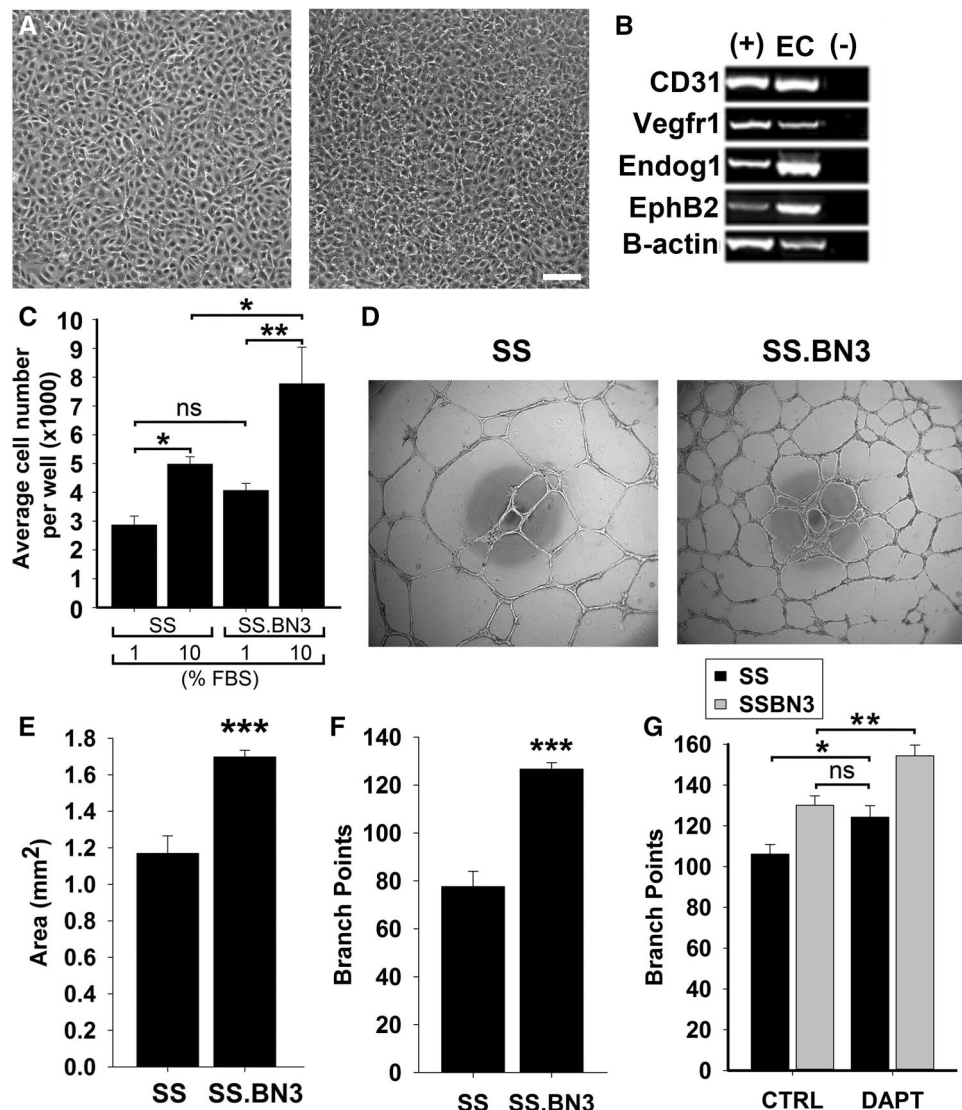
($n = 4$) and SS.BN3$^{IL2R\gamma}$ ($n = 4$). This revealed 541 DE genes and 489 DE transcript isoforms in the host TME of SS.BN3$^{IL2R\gamma}$ tumors compared with SS$^{IL2R\gamma}$ (Supplemental Tables 1, 2). DE genes and transcript isoforms were significantly enriched on RNO3 compared to the genome-wide average ($p < 0.001$; Fig. 4a–d), as were the distributions of p values for RNO3 versus the rest of the genome (Fig. 4e, f).
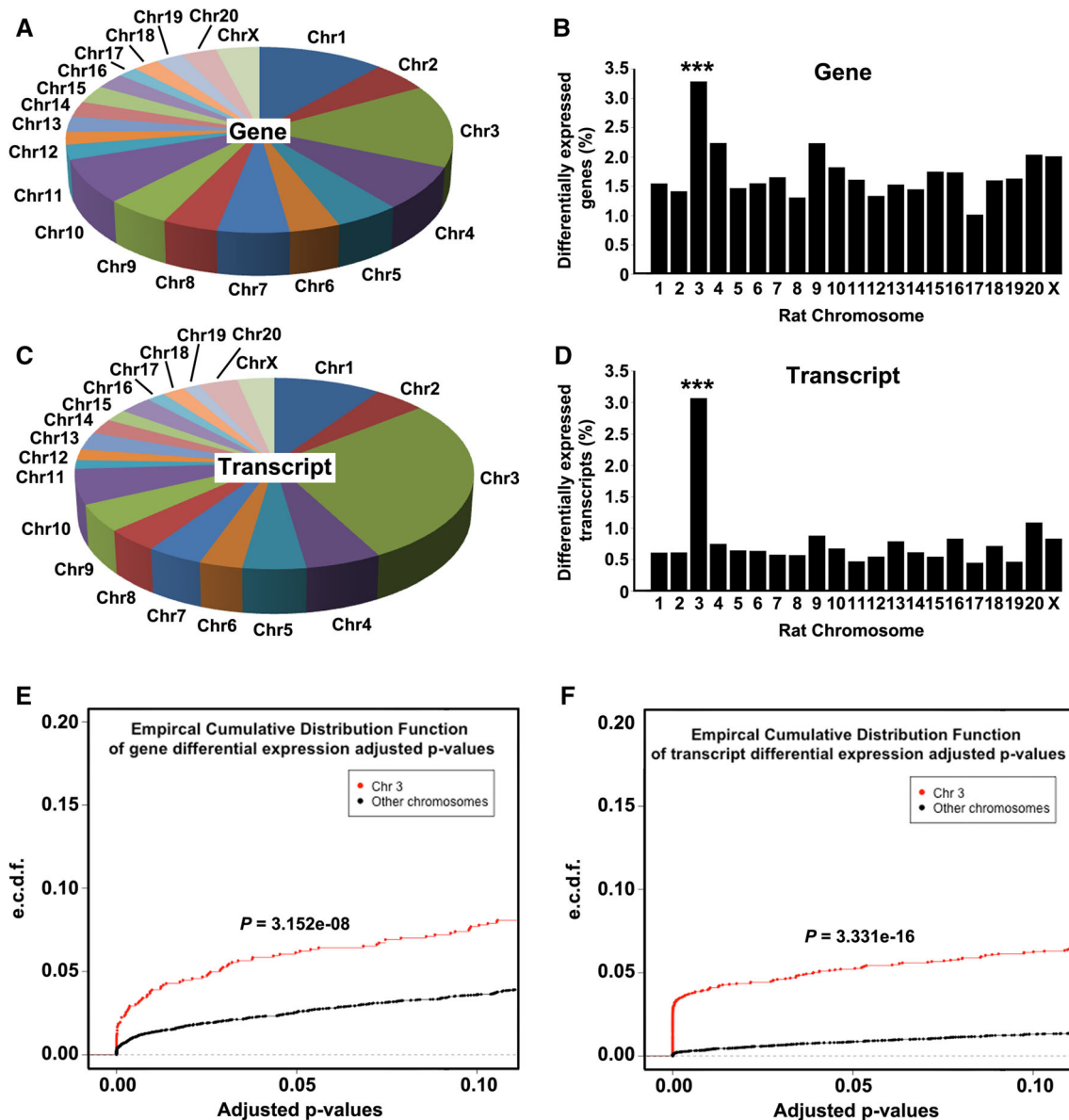
Gene ontology (GO) analysis of the merged list of DE genes and transcript isoforms using ingenuity pathway analysis (IPA) revealed that the most enriched GO cluster was related to vascular development and angiogenesis (Supplemental Tables 5, 6). Of the DE candidates in the vascular development and angiogenesis GO, only DLL4 was previously linked with altered vascular branching that leads to nonproductive angiogenesis and tumor growth inhibition [12, 24–28], which matches the phenotypes

Fig. 4 Localization of differentially expressed genes and transcripts in the TME of SS.BN3$^{IL2R\gamma}$ ($n = 4$) and SS$^{IL2R\gamma}$ ($n = 4$) rats, as determined by SSRS. **a** Chromosomal distribution of the 541 differentially expressed genes in the TME of SS.BN3$^{IL2R\gamma}$ rats compared with the SS$^{IL2R\gamma}$. **b** Differentially expressed genes from panel (**a**) presented as differentially expressed genes per chromosome normalized to total number of genes per chromosome. **c** Chromosomal distribution of the 489 differentially expressed transcript isoforms in the TME of SS.BN3$^{IL2R\gamma}$ rats compared with the SS$^{IL2R\gamma}$. **d** Differentially expressed transcript isoforms from panel (**c**) presented as differentially expressed transcript isoforms per chromosome normalized to the total number of transcript isoforms per chromosome. ***$p < 0.001$, as determined by Fisher's exact test. Distributions of adjusted p values for differentially expressed genes (**e**) and differentially expressed transcripts (**f**) on RNO3 versus the rest of the rat genome were tested by a two-sample Kolmogorov–Smirnov test

observed in the SS.BN3$^{IL2R\gamma}$ CXM model (Figs. 1, 2, 3, 4). Expression of DLL4 protein on tumor blood vessels was also reduced in 231^{Luc+} and HCC1806-RR tumors implanted in SS.BN3$^{IL2R\gamma}$ rats compared with SS$^{IL2R\gamma}$ tumors (Fig. 5c, d). Compared with SS$^{IL2R\gamma}$ tumors, the density DLL4$^+$ blood vessels decreased 50–60% in 231^{Luc+} and HCC1806-RR tumors implanted in SS.BN3$^{IL2R\gamma}$ rats (Fig. 5e, f), despite a nearly twofold increase in density of total CD31$^+$ tumor blood vessels (Fig. 2a–d). Additionally, blockade of the DLL4 pathway in SS-derived EC by the γ-secretase inhibitor, DAPT [24], enhanced in vitro tube formation (124 ± 6 branchpoints; $p < 0.05$) compared with control-treated EC (106 ± 5 branchpoints) (Supplemental Fig. 3), suggesting that inhibition of the DLL4 pathway increases vascular branching, as has been demonstrated previously [12, 24–28].

DLL4 co-localizes within a host TME modifier locus of tumor growth and angiogenesis

We next attempted to test the molecular role of DLL4 in our model by shRNA-mediated knockdown; however, we were unable to identify shRNA reagents that reproducibly downregulated DLL4 expression in the rat. Thus, we instead mapped the host TME modifier(s) (e.g., DLL4) on RNO3 using three SS.BN3$^{IL2R\gamma}$ congenic xenograft host strains (line A$^{IL2R\gamma}$, line B$^{IL2R\gamma}$, and line C$^{IL2R\gamma}$). As shown in Fig. 6, 231^{Luc+} or HCC1806-RR cells were orthotopically implanted into the MFP of SS$^{IL2R\gamma}$, SS.BN3$^{IL2R\gamma}$, line A$^{IL2R\gamma}$, line B$^{IL2R\gamma}$, and line C$^{IL2R\gamma}$. We found that 231^{Luc+} tumors implanted SS$^{IL2R\gamma}$ (6680 ± 719 mm^3, $n = 10$) were significantly larger than SS.BN3$^{IL2R\gamma}$ consomic (2714 ± 149 mm^3, $p < 0.05$, $n = 26$) and line A$^{IL2R\gamma}$
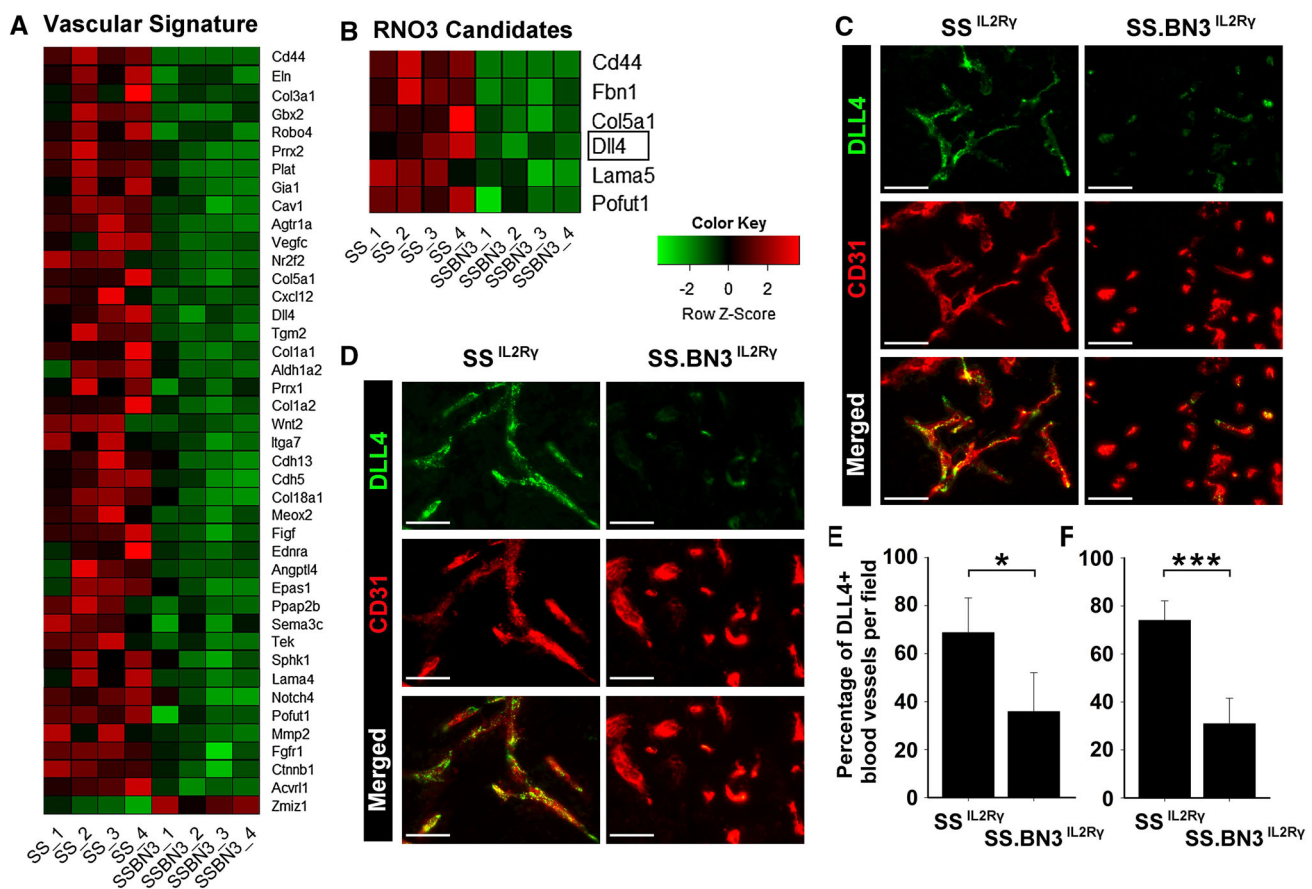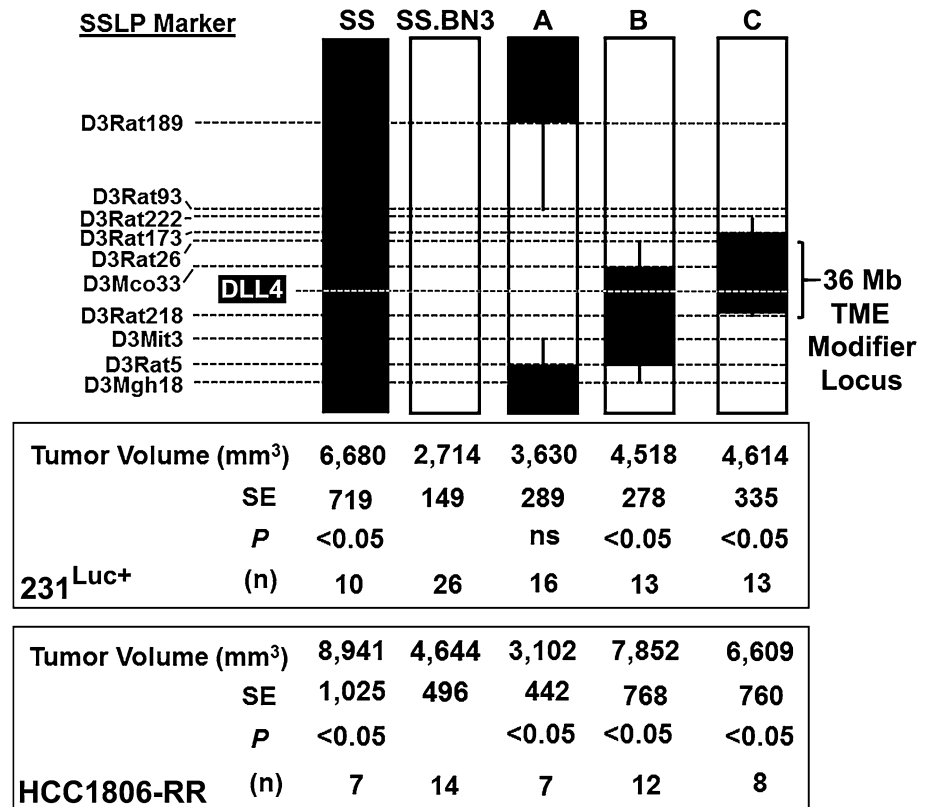

Fig. 5 DLL4 is a candidate TME modifier that is downregulated in the vasculature of SS.BN3$^{IL2R\gamma}$ tumors compared with SS$^{IL2R\gamma}$. **a** Heatmap of the 43 differentially expressed mRNAs (FDR < 0.1) that make up the blood vasculature GO cluster. **b** Heatmap of the six differentially expressed mRNAs in the blood vasculature GO cluster that reside on RNO3. **c, d** Expression of DLL4 protein (*green*) on CD31$^+$ blood vessels (*red*) was assessed by dual immunofluorescent staining of 231^{Luc+} (**c**) and HCC1806-RR (**d**) tumors implanted in SS$^{IL2R\gamma}$ and SS.BN3$^{IL2R\gamma}$ rats. Note that DLL4 is co-localized to CD31$^+$ tumor blood vessels and is downregulated in SS.BN3$^{IL2R\gamma}$ tumors compared to SS$^{IL2R\gamma}$. **e, f** Quantification of the percentage of DLL4$^+$ blood vessels in 231^{Luc+} (**e**) and HCC1806-RR (**f**) tumors implanted in SS$^{IL2R\gamma}$ and SS.BN3$^{IL2R\gamma}$ rats ($n = 5$–8 tumors per group). Data are presented as mean $\pm$ SEM. $*p < 0.05$ and $***p < 0.001$, as determined by Student unpaired t test

Fig. 6 Schematic representation of the SS.BN3$^{IL2R\gamma}$ congenic strains that were generated by introgressing segments of BN chromosome 3 (*black*) into the genetic background of the parental SS$^{IL2R\gamma}$ strain (*white*) by marker-assisted breeding. *Thin black bars* represent confidence intervals, which are chromosomal regions that could be BN or SS. The position of *DLL4* (chr3: 111,135,011–111,146,746 bp) and the 36 Mb host TME modifier locus (chr3: 95,176,874–131,051,652 bp). Tumor volumes were measured at 24 days post-implantation of the 231^{Luc+} and HCC1806-RR TNBC cell lines. Data are presented as mean ± SEM. *p < 0.05, as determined by 1-way ANOVA followed by Holm–Sidak post hoc test
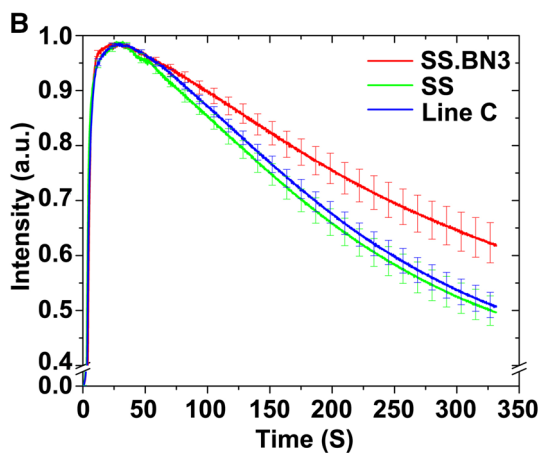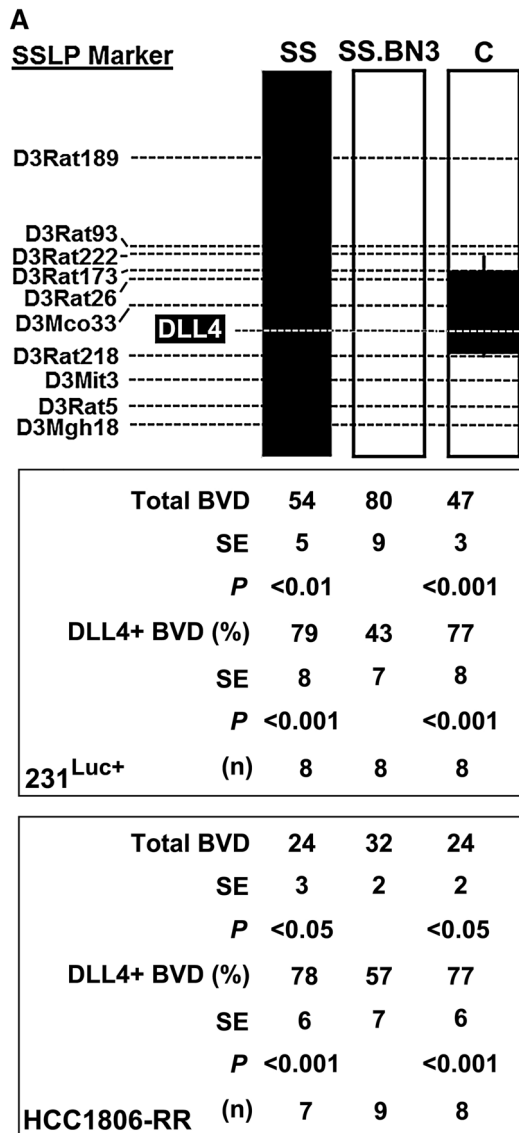

SSLP Marker		SS	SS.BN3	A	B	C
Tumor Volume (mm³)		6,680	2,714	3,630	4,518	4,614
	SE	719	149	289	278	335
	P	<0.05		ns	<0.05	<0.05
231^{Luc+}	(n)	10	26	16	13	13

Tumor Volume (mm³)		8,941	4,644	3,102	7,852	6,609
	SE	1,025	496	442	768	760
	P	<0.05		<0.05	<0.05	<0.05
HCC1806-RR	(n)	7	14	7	12	8

(3630 ± 289 mm³, $p < 0.05$, $n = 16$) tumors at 24 days post-implantation, whereas the volumes of 231^{Luc+} tumors implanted in line B$^{IL2R\gamma}$ (4518 ± 278 mm³, $n = 13$) and line C$^{IL2R\gamma}$ (4614 ± 335 mm³, $n = 13$) did not significantly differ from SS$^{IL2R\gamma}$ (Fig. 6). Similarly, HCC1806-RR tumor growth was significantly inhibited in the SS.BN3$^{IL2R\gamma}$ consomic and line A$^{IL2R\gamma}$ compared with SS$^{IL2R\gamma}$, line B$^{IL2R\gamma}$, and line C$^{IL2R\gamma}$ (Fig. 6). By exclusion mapping, these data suggest that host TME modifier(s) of TNBC growth reside within a 36 Mb locus on RNO3 (Chr3: 95–131 Mb), a region that contains DLL4 (Fig. 5a–c).

We next assessed whether the host TME modifier locus on RNO3 (Chr3: 95–131 Mb) altered the tumor vascular density and function, and vascular-specific DLL4 expression. Compared with the CD31$^+$ vessel density of SS.BN3$^{IL2R\gamma}$ tumors (80 ± 9 vessels/field), the 231^{Luc+} tumors implanted in SS$^{IL2R\gamma}$ (54 ± 5 vessels/field; $p < 0.01$) and line C$^{IL2R\gamma}$ (47 ± 3 vessels/field; $p < 0.001$) had significantly decreased tumor vascular density (Fig. 7a). Likewise, HCC1806-RR tumor vascular density was significantly higher in the SS.BN3$^{IL2R\gamma}$ consomic compared with SS$^{IL2R\gamma}$ and line C$^{IL2R\gamma}$ (Fig. 7a). For both TNBC lines, the density of CD31$^+$/DLL4$^+$ double-positive vessels in SS.BN3$^{IL2R\gamma}$ tumors was significantly less ($p < 0.05$) than SS$^{IL2R\gamma}$ and line C$^{IL2R\gamma}$ tumors, despite significantly increased density of CD31$^+$ blood vessels in

SS.BN3$^{IL2R\gamma}$ tumors (Fig. 7a). Finally, analysis of tumor vascular function showed a delayed washout of ICG dye in 231^{Luc+} tumors implanted in SS.BN3$^{IL2R\gamma}$ compared with SS$^{IL2R\gamma}$ and line C$^{IL2R\gamma}$ (Fig. 7b). Collectively, these data suggest that the host TME modifier(s) of tumor growth inhibition and nonproductive angiogenesis reside within the 36 Mb locus on RNO3 (Chr3: 95–131 Mb), which co-localizes with differential expression of DLL4.

Discussion

Perfusion MRI analysis of tumor vascular function can be used to predict more aggressive histopathologic features and outcomes in breast cancer patients, such as tumor grade [6], response to neoadjuvant chemotherapy [7–10], and overall survival [11]. However, the genetic and molecular mechanism(s) underlying the tumor vascular changes and the prognostic factors remain poorly understood. Here, we present a novel experimental model with key vascular phenotypes that recapitulate perfusion characteristics that may correlate with the aggressiveness of human breast cancers. Compared with the SS.BN3$^{IL2R\gamma}$ strain, tumor growth in the SS$^{IL2R\gamma}$ rat was significantly more aggressive and this coincided with a rapid washout on DCE-MRI that has been associated with higher grade of tumors [6] and worse overall survival prognosis in human

A

SSLP Marker

	SS	SS.BN3	C

D3Rat189

D3Rat93
D3Rat222
D3Rat173
D3Rat26
D3Mco33 — DLL4
D3Rat218
D3Mit3
D3Rat5
D3Mgh18

	SS	SS.BN3	C
Total BVD	54	80	47
SE	5	9	3
P	<0.01		<0.001
DLL4+ BVD (%)	79	43	77
SE	8	7	8
P	<0.001		<0.001
231[Luc+] **(n)**	8	8	8

	SS	SS.BN3	C
Total BVD	24	32	24
SE	3	2	2
P	<0.05		<0.05
DLL4+ BVD (%)	78	57	77
SE	6	7	6
P	<0.001		<0.001
HCC1806-RR (n)	7	9	8

B

◄**Fig. 7** Congenic mapping of vascular density and function, which coincide with altered vascular-specific DLL4 protein expression. **a** Analysis of the mean density of CD31^{+} blood vessels per 200× field ($n = 3$ images per tumor) and the percentage of CD31^{+}/DLL4^{+} double-positive blood vessels per 400× field ($n = 3$ images per tumor). Data are presented as mean ± SEM. *$p < 0.05$, **$p < 0.01$, and ***$p < 0.001$, as determined by 1-way ANOVA followed by Holm–Sidak post hoc test. **b** Tumor vascular function was assessed by near infrared imaging of circulating ICG dye in 231[Luc+] tumors at 10 days post-implantation

patients [11]. These findings, combined with morphometric and functional analyses of the blood vasculature (Figs. 2, 3), indicate that host genetic modifier(s) on RNO3 alter vascular structure and function in the SS.BN3[IL2Rγ] CXM rat strain. These vascular alterations were also detected at the molecular level by SSRS and immunofluorescent imaging, which revealed an altered vascular gene network that was highlighted by dysregulation of DLL4 in the TME of SS.BN3[IL2Rγ] tumors (Fig. 5). By congenic mapping, we localized a host TME modifier locus (Chr3: 95–131 Mb) that contains DLL4 and was correlated with the tumor growth and vascular phenotypes that were observed at the consomic level (Figs. 6, 7). Collectively, these data suggest that DLL4 is likely a host TME modifier of breast cancer in the SS.BN3[IL2Rγ] CXM strain, albeit further congenic mapping or gene-editing is necessary to exclude other potential candidate(s) in the region and isolate the causative variant(s).

It is notable that the DLL4 pathway is a master regulator of angiogenic vascular patterning [12, 24–31] and inhibition of DLL4 attenuates tumor growth and progression by eliciting nonproductive angiogenesis (i.e., a higher density of poorly functioning vasculature) [12, 24–28], which is similar to the phenotypes observed in the SS.BN3[IL2Rγ] tumors. During angiogenesis, VEGF upregulates DLL4 expression on the vascular tip cells and DLL4 then activates NOTCH1 signaling in the adjacent endothelial cells to suppress aberrant tip cell formation and excessive vascular branching [25, 29–31]. In the SS.BN3[IL2Rγ] model, we observed a TME-specific decrease in expression of DLL4 that coincided with nonfunctional angiogenesis and decreased growth of SS.BN3[IL2Rγ] tumors. Congenic mapping further localized the host TME locus on RNO3 (Chr3: 95–131 Mb) that contains DLL4 and modified DLL4 expression (Fig. 7), which coincided with altered tumor growth (Fig. 6) and altered tumor vascular density and function (Fig. 7). Although these data due not exclude the possibility of other TME modifier(s) within the TME locus on RNO3 (Chr3: 95–131 Mb), the downregulation of

DLL4 and the observations in SS.BN3$^{IL2R\gamma}$ tumors that phenocopy the inhibition of DLL4 [12, 24–28] suggest that the DLL4 pathway is a plausible candidate on RNO3. However, these findings do not exclude additional host TME modifier(s) on RNO3 that might interact with the DLL4 pathway (e.g., upstream or downstream mediators) or function independently of the DLL4 pathway. The next step to verifying the causative DLL4 allele(s) or discovering new candidates will be to further map the TME modifier(s) using smaller subcongenic strains or gene-editing approaches.

Tumor angiogenesis is a highly coordinated process that is necessary for growth and progression of breast cancer [23, 32]. A denser tumor vasculature is largely correlated with increased tumor growth and hematogenous metastasis, which is thought to be due to enhanced supply of oxygen and nutrients to the tumor and by providing more routes for metastatic dissemination [33]. Although many initial studies focused on the prognostic value of tumor blood vessel density [33, 34], it is increasingly evident that functionality of the tumor vasculature is also an important predictor of patient outcomes (e.g., tumor grade [6], response to neoadjuvant chemotherapy [7–10], and overall survival [11]). A rapid accumulation and washout of Gd+ that is associated with higher grade of tumors [6] and worse overall survival prognosis in human patients [11] is thought to reflect a denser network of tumor vessels that facilitate tumor growth and metastasis. However, our data suggest that the predictive values of tumor vascular density and function might not always coincide. Although the vascular density was increased in SS.BN3$^{IL2R\gamma}$ tumors compared with SS$^{IL2R\gamma}$ tumors (Fig. 2a–e) [5], this correlated negatively with tumor growth (Fig. 1) and the DCE-MRI washout curves that were indicative of less aggressive breast cancer (Fig. 2). Collectively, these data suggest that germline genetic variants in the host TME can modify the pathways that regulate tumor vascular density and function (e.g., the DLL4 pathway), which ultimately impacts tumor growth and disease progression. Identifying these host TME modifiers will likely improve the accuracy of breast cancer patient prognosis and potentially provide novel therapeutic targets for treating breast cancer patients.

Compliance with ethical standards

References

1. Quail DF, Joyce JA (2013) Microenvironmental regulation of tumor progression and metastasis. Nat Med 19(11):1423–1437
2. Polyak K, Kalluri R (2010) The role of the microenvironment in mammary gland development and cancer. Cold Spring Harbor Perspect Biol 2(11):a003244
3. Cook LM, Hurst DR, Welch DR (2011) Metastasis suppressors and the tumor microenvironment. Semin Cancer Biol 21(2):113–122
4. McAllister SS, Weinberg RA (2010) Tumor-host interactions: a far-reaching relationship. J Clin Oncol 28(26):4022–4028
5. Flister MJ, Endres BT, Rudemiller N, Sarkis AB, Santarriaga S, Lemke A, Roy I, Geurts AM, Moreno C, Ran S et al (2014) CXM—a new tool for mapping breast cancer risk in the tumor microenvironment. Cancer Res 74(22):6419–6429
6. Han M, Kim TH, Kang DK, Kim KS, Yim H (2012) Prognostic role of MRI enhancement features in patients with breast cancer: value of adjacent vessel sign and increased ipsilateral whole-breast vascularity. AJR 199(4):921–928
7. Craciunescu OI, Blackwell KL, Jones EL, Macfall JR, Yu D, Vujaskovic Z, Wong TZ, Liotcheva V, Rosen EL, Prosnitz LR et al (2009) DCE-MRI parameters have potential to predict response of locally advanced breast cancer patients to neoadjuvant chemotherapy and hyperthermia: a pilot study. Int J Hyperth 25(6):405–415
8. Ah-See ML, Makris A, Taylor NJ, Harrison M, Richman PI, Burcombe RJ, Stirling JJ, d'Arcy JA, Collins DJ, Pittam MR et al (2008) Early changes in functional dynamic magnetic resonance imaging predict for pathologic response to neoadjuvant chemotherapy in primary breast cancer. Clin Cancer Res 14(20):6580–6589
9. Jia WR, Tang L, Wang DB, Chai WM, Fei XC, He JR, Chen M, Wang WP (2016) Three-dimensional contrast-enhanced ultrasound in response assessment for breast cancer: a comparison with dynamic contrast-enhanced magnetic resonance imaging and pathology. Sci Rep 6:33832
10. Sun YS, He YJ, Li J, Li YL, Li XT, Lu AP, Fan ZQ, Cao K, Ouyang T (2016) Predictive value of DCE-MRI for early evaluation of pathological complete response to neoadjuvant chemotherapy in resectable primary breast cancer: a single-center prospective study. Breast 30:80–86
11. Heldahl MG, Bathen TF, Rydland J, Kvistad KA, Lundgren S, Gribbestad IS, Goa PE (2010) Prognostic value of pretreatment

dynamic contrast-enhanced MR imaging in breast cancer patients receiving neoadjuvant chemotherapy: overall survival predicted from combined time course and volume analysis. Acta Radiol 51(6):604–612

12. Noguera-Troise I, Daly C, Papadopoulos NJ, Coetzee S, Boland P, Gale NW, Lin HC, Yancopoulos GD, Thurston G (2006) Blockade of Dll4 inhibits tumour growth by promoting non-productive angiogenesis. Nature 444(7122):1032–1037

13. Flister MJ, Hoffman MJ, Reddy P, Jacob HJ, Moreno C (2013) Congenic mapping and sequence analysis of the Renin locus. Hypertension 61(4):850–856

14. Hoffman MJ, Flister MJ, Nunez L, Xiao B, Greene AS, Jacob HJ, Moreno C (2013) Female-specific hypertension Loci on rat chromosome 13. Hypertension 62(3):557–563

15. Volk LD, Flister MJ, Bivens CM, Stutzman A, Desai N, Trieu V, Ran S (2008) Nab-paclitaxel efficacy in the orthotopic model of human breast cancer is significantly enhanced by concurrent anti-vascular endothelial growth factor A therapy. Neoplasia 10(6):613–623

16. Volk-Draper LD, Rajput S, Hall KL, Wilber A, Ran S (2012) Novel model for basaloid triple-negative breast cancer: behavior in vivo and response to therapy. Neoplasia 14(10):926–942

17. Walker EJ, Shen F, Young WL, Su H (2011) Cerebrovascular casting of the adult mouse for 3D imaging and morphological analysis. J Vis Exp 57:e2958–e2958

18. Prisco AR, Bukowy JD, Hoffmann BR, Karcher JR, Exner EC, Greene AS (2014) Automated quantification reveals hyper-glycemia inhibits endothelial angiogenic function. PLoS ONE 9(4):e94599

19. Langmead B, Salzberg SL (2012) Fast gapped-read alignment with Bowtie 2. Nat Methods 9(4):357–359

20. Roberts A, Pachter L (2013) Streaming fragment assignment for real-time analysis of sequencing experiments. Nat Methods 10(1):71–73

21. Anders S, Huber W (2010) Differential expression analysis for sequence count data. Genome Biol 11(10):R106

22. Flister MJ, Volk LD, Ran S (2011) Characterization of Prox1 and VEGFR-3 expression and lymphatic phenotype in normal organs of mice lacking p50 subunit of NF-kappaB. Microcirculation 18(2):85–101

23. Hanahan D, Folkman J (1996) Patterns and emerging mecha-nisms of the angiogenic switch during tumorigenesis. Cell 86(3):353–364

24. Scehnet JS, Jiang W, Kumar SR, Krasnoperov V, Trindade A, Benedito R, Djokovic D, Borges C, Ley EJ, Duarte A et al (2007) Inhibition of Dll4-mediated signaling induces proliferation of immature vessels and results in poor tissue perfusion. Blood 109(11):4753–4760

25. Hellstrom M, Phng LK, Hofmann JJ, Wallgard E, Coultas L, Lindblom P, Alva J, Nilsson AK, Karlsson L, Gaiano N et al (2007) Dll4 signalling through Notch1 regulates formation of tip cells during angiogenesis. Nature 445(7129):776–780

26. Xu Z, Wang Z, Jia X, Wang L, Chen Z, Wang S, Wang M, Zhang J, Wu M (2016) MMGZ01, an anti-DLL4 monoclonal antibody, promotes nonfunctional vessels and inhibits breast tumor growth. Cancer Lett 372(1):118–127

27. Ridgway J, Zhang G, Wu Y, Stawicki S, Liang WC, Chanthery Y, Kowalski J, Watts RJ, Callahan C, Kasman I et al (2006) Inhibition of Dll4 signalling inhibits tumour growth by deregu-lating angiogenesis. Nature 444(7122):1083–1087

28. Hoey T, Yen WC, Axelrod F, Basi J, Donigian L, Dylla S, Fitch-Bruhns M, Lazetic S, Park IK, Sato A et al (2009) DLL4 blockade inhibits tumor growth and reduces tumor-initiating cell frequency. Cell Stem Cell 5(2):168–177

29. Suchting S, Freitas C, le Noble F, Benedito R, Breant C, Duarte A, Eichmann A (2007) The notch ligand Delta-like 4 negatively regulates endothelial tip cell formation and vessel branching. Proc Natl Acad Sci USA 104(9):3225–3230

30. Siekmann AF, Lawson ND (2007) Notch signalling limits angiogenic cell behaviour in developing zebrafish arteries. Nature 445(7129):781–784

31. Lobov IB, Renard RA, Papadopoulos N, Gale NW, Thurston G, Yancopoulos GD, Wiegand SJ (2007) Delta-like ligand 4 (Dll4) is induced by VEGF as a negative regulator of angiogenic sprouting. Proc Natl Acad Sci USA 104(9):3219–3224

32. Bergers G, Benjamin LE (2003) Tumorigenesis and the angio-genic switch. Nat Rev Cancer 3(6):401–410

33. Nico B, Benagiano V, Mangieri D, Maruotti N, Vacca A, Ribatti D (2008) Evaluation of microvascular density in tumors: pro and contra. Histol Histopathol 23(5):601–607

34. Weidner N, Semple JP, Welch WR, Folkman J (1991) Tumor angiogenesis and metastasis–correlation in invasive breast car-cinoma. N Engl J Med 324(1):1–8